

Designing Structural Motifs for Clickamers: Exploiting the 1,2,3-Triazole Moiety to Generate Conformationally Restricted Molecular Architectures

Denise Zornik,^[a] Robert M. Meudtner,^[a] Tamer El Malah,^[a] Christina M. Thiele,^[b] and Stefan Hecht*^[a]

Abstract: Noncovalent interactions, especially hydrogen-bonding interactions as well as electrostatic forces, confined within one macromolecule are the key to designing foldamers that adopt well-defined conformations in solution. In the context of significant recent activities in the area of triazole-connected foldamers, so-called clickamers, we present a fundamental study that compares various model compounds that bear adjacent N-, O-, or F-heteroatom substituents. The interplay of attractive and repulsive interactions leads to rotational constraints around the single

bonds attached to both the 1- and 4-positions of the 1,2,3-triazole moiety and should therefore be able to induce well-defined conformational preferences in higher oligomers and polymers, that is, foldamers. Various compounds were synthesized and characterized with regard to their preferred conformations in all three aggregation states—that is, in the gas phase, in solu-

Keywords: click chemistry • conformation analysis • foldamers • supramolecular chemistry • triazoles

tion as well as in the solid state—by employing DFT calculations, NMR spectroscopic experiments, and X-ray crystallography, respectively. On the basis of the thus-obtained general understanding of the conformational behavior of the individual connection motifs, heterostructures were prepared from different motifs without affecting their distinct folding characteristics. Therefore, this work provides a kind of foldamer construction kit, which should enable the design of various clickamers with specific shape and incorporated functionality.

Introduction

In recent years, a great deal of scientific effort has been devoted towards understanding general structure–function relationships in synthetic macro- and supramolecules and also exploiting this insight to improve their properties for future applications. The key question in designing novel soft materials relates to the controlled spatial arrangement of functional entities (most commonly monomer units) for which noncovalent approaches—that is, self-assembly of small molecules^[1] or block copolymers^[2] and supramolecular poly-

mers^[3]—as well as covalent approaches—that is, dendrimers^[4] and foldamers^[5]—and combinations of both have been used.^[6] This hierarchical bottom-up strategy to assemble complex functional systems is, not surprisingly, mainly inspired by nature's strategies, exemplified by protein structure formation. Here, the primary structure encoding a (hetero)sequence of monomer units is translated to a defined secondary structure, which is further organized into tertiary folds. Both of these levels of organization are caused by intramolecular noncovalent interactions within a covalently connected backbone, which in general is referred to as a foldamer.^[5] Nature utilizes primarily peptides for this task; however, for nonbiological materials, thermally and chemically more robust backbones are desired. Aromatic—as opposed to aliphatic—amide foldamers offer such enhanced stability,^[7] and several groups have successfully designed examples of these backbones.^[8] In these systems, folding—in most cases into a helical structure—is induced by geometrical constraints rather than environmental effects.^[9] These constraints are generated by various stabilizing and destabilizing interactions between adjacent aromatic monomers units connected by the rigid and *trans*-configured amide linkage.^[8]

[a] Dipl.-Chem. D. Zornik, Dr. R. M. Meudtner, Dipl.-Chem. T. El Malah, Prof. Dr. S. Hecht
Department of Chemistry, Humboldt-Universität zu Berlin
Brook-Taylor-Strasse 2, 12489 Berlin (Germany)
Fax: (+49)30-2093-6940
E-mail: sh@chemie.hu-berlin.de

[b] Dr. C. M. Thiele
Clemens Schöpf Institut für Organische Chemie
Technische Universität Darmstadt
Petersenstrasse 22, 64287 Darmstadt (Germany)

Supporting information for this article is available on the WWW under <http://dx.doi.org/10.1002/chem.201002491>.

These interactions can generate conformationally biased bent connections, which at a critical length lead either to a folding into a three-dimensional helical structure or into a two-dimensional zigzag linear tape structure (Figure 1). The amide linkage is by far the most popular connection^[10] of aromatic monomer units in these foldamers. However, substi-

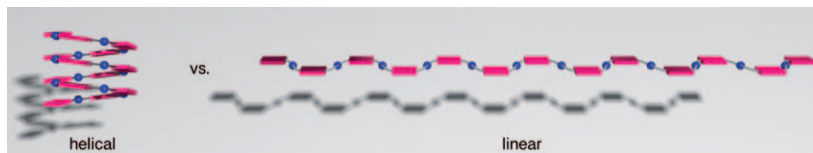


Figure 1. Illustration of conformational preferences within rigid aromatic foldamers that lead to either 3D helix or 2D linear tape formation (aromatic units shown in red, bent connections shown in blue).

tution of the amide functionalities by the isosteric 1,2,3-triazole moieties^[11] offers both, a synthetic advantage due to the orthogonal and high-yielding coupling chemistry as well as new structural and electronic features that arise from the triazole ring. By exploiting the highly efficient copper-catalyzed “click” reaction not only to efficiently connect monomer units but also to incorporate the triazole unit to induce secondary structure formation, we have recently developed the 2,6-bis(1-aryl-1,2,3-triazol-4-yl)pyridine (BTP) motif^[12,13] and investigated BTP-derived scaffolds for responsive folding in solution,^[14] as ligands^[15] and metallosupramolecular gels,^[16] as well as at the liquid–solid interface.^[17] To apply our strategy for the design of new backbones, we have engaged in a detailed study of various 1,2,3-triazole-connected (hetero)aromatic systems. Here, we report on the synthesis of these new folding motifs and discuss the influence of different heteroatoms—that is, N-, O-, F-substitution—on the conformational preference about both the N(1)-aryl of the triazole as well as the C(4)-aryl bonds.

Results and Discussion

General design considerations: In our previous work,^[12,14–17] solely the BTP motif was used, which offers conformational restriction only about the C(4)-aryl connection, readily achieved by means of a click reaction of bis(*ortho*-ethynyl)pyridines with aromatic azides. Initial attempts to also bias the N(1)-aryl connection failed because bis(*ortho*-azido)pyridines could not be prepared. We therefore sought to incorporate other (hetero)aromatic units to bias conformation about the N(1)- as well as C(4)-linkages. By assuming only two possible flat conformations due to π conjugation—that is, *syn* and *anti* (Scheme 1, top)—attractive interactions of the incorporated heteroatoms with the triazole proton on C(5) as well as the *ortho* protons with N(2) or N(3) are supposed to favor the *anti* conformation. On the other hand, the *syn* conformation should be strongly disfavored due to repulsive interactions of the heteroatoms (X) with the N(2) and N(3) atoms of the central triazole moiety and steric repulsion between the *ortho*-protons and the triazole proton

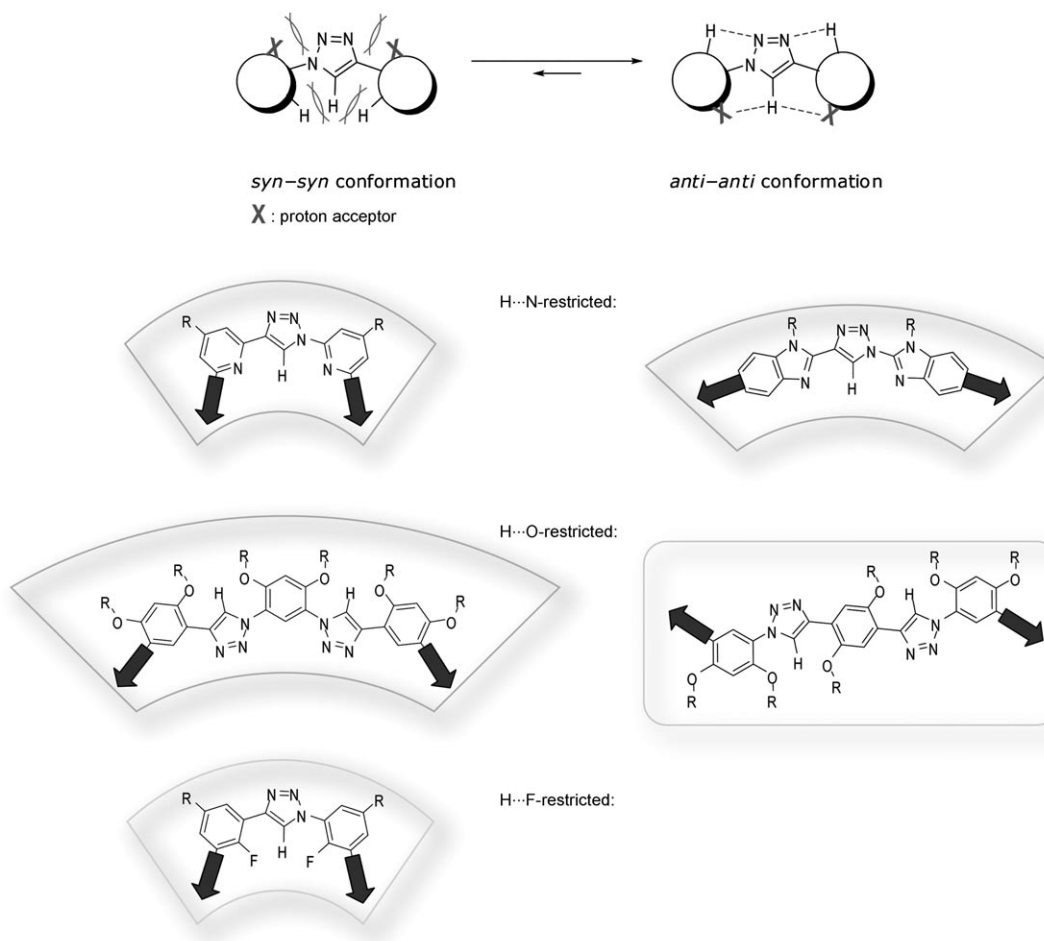
on C(5). We have investigated various types of heteroatom substitution, that is, nitrogen, oxygen, and fluorine, known to engage in considerably strong hydrogen-bonding-type interactions. In addition to N-containing heteroaromatics—that is, pyridines and benzimidazoles—*ortho*-alkoxy-substituted as well as *ortho*-fluorine-substituted phenyl moieties have been explored (Scheme 1). Based upon the relative orientation of the heteroatoms adjacent to the triazole ring, either progressively kinked or zigzag structures can be formed, thereby resulting in helices and linear strands, respectively.

Conformational constraints based on H \cdots N interactions:

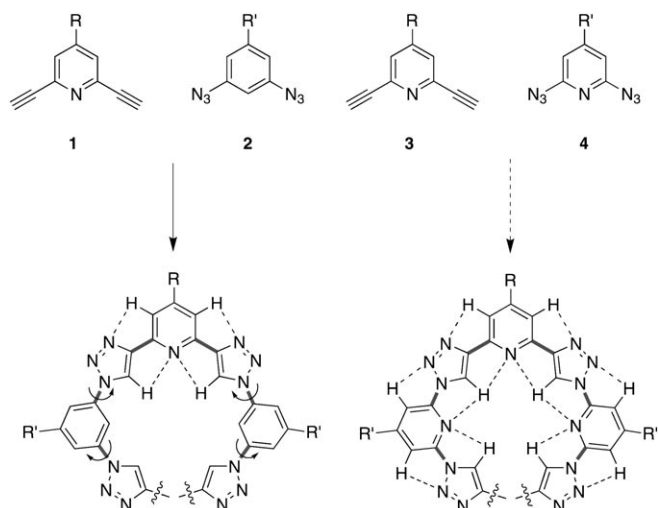
Our original design of clickamers^[14] based on the BTP motif offers conformational constraints only about the C(4)-triazolyl–2-pyridyl bond, whereas the N(1)-triazolyl–phenyl bond displays no preference for either the *syn* or the *anti* conformation (Scheme 2, left). Hence, folding involves rigidified kinked BTP moieties connected by flexible *meta*-phenylene hinges.^[14,16] To generate fully rigidified helices, *ortho*-pyridyl moieties were introduced by means of click chemistry that involved the corresponding 2-azidopyridines, which should bias the conformation about the N(1)-triazolyl–2-pyridyl bond (Scheme 2, right).

2-Azidopyridine derivative **8a** (Scheme 3) could successfully be synthesized from nitroxide **5**. Although the compound mostly exists as the tetrazole tautomer **8b**,^[18] the subsequent click reaction with the previously described 2,6-bis(ethynyl)pyridine **9** was successful and gave the desired product **10**. Please note that the yields of the click reactions given throughout this article are not optimized and do not necessarily reflect inefficient reactions but rather troublesome purification of the target compounds, often caused by their low solubility in combination with residual traces of copper species. Presumably due to the less ordered tri(ethylene glycol) groups, no single crystals of compound **10** could be grown for detailed structural analysis and hence *n*-hexyl side chains were introduced by a two-step saponification–esterification sequence to yield **12**. Indeed, single crystals could be obtained by slow diffusion of petroleum ether into a solution of **12** in acetone. The corresponding single crystal structure (Figure 2) displays the expected horseshoelike, planar *anti*–*anti* conformation of both linkages, that is, the N(1)–C of the triazoles as well as the C(4)–C connectivities of the triazoles. Due to deviations in bond lengths and dihedral angles (Figure 2), the molecule possesses only little symmetry yet can still be considered planar as the absolute angle variations are rather small.

Unfortunately, available synthetic strategies could only be applied to introduce one azide group in the *ortho* position of the pyridine heterocycle. Both synthesis of the 2,6-bisazidopyridine derivative as well as extension of the initially prepared structure **12** at its termini by repeated introduction



Scheme 1. Design of clickamer motifs that involve heteroatom substitution, which illustrates general conformational preferences and the resulting secondary structure of the various investigated foldamer motifs discussed in this article.



Scheme 2. Foldamer motifs based on 2,6-diethynylpyridine: Partially restricted conformation by oligomerization with 1,3-bisazidobenzene (left) versus fully restricted conformation by oligomerization with 2,6-bisazidopyridines (right).

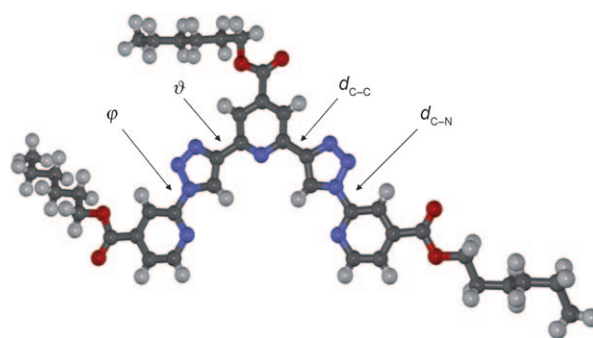
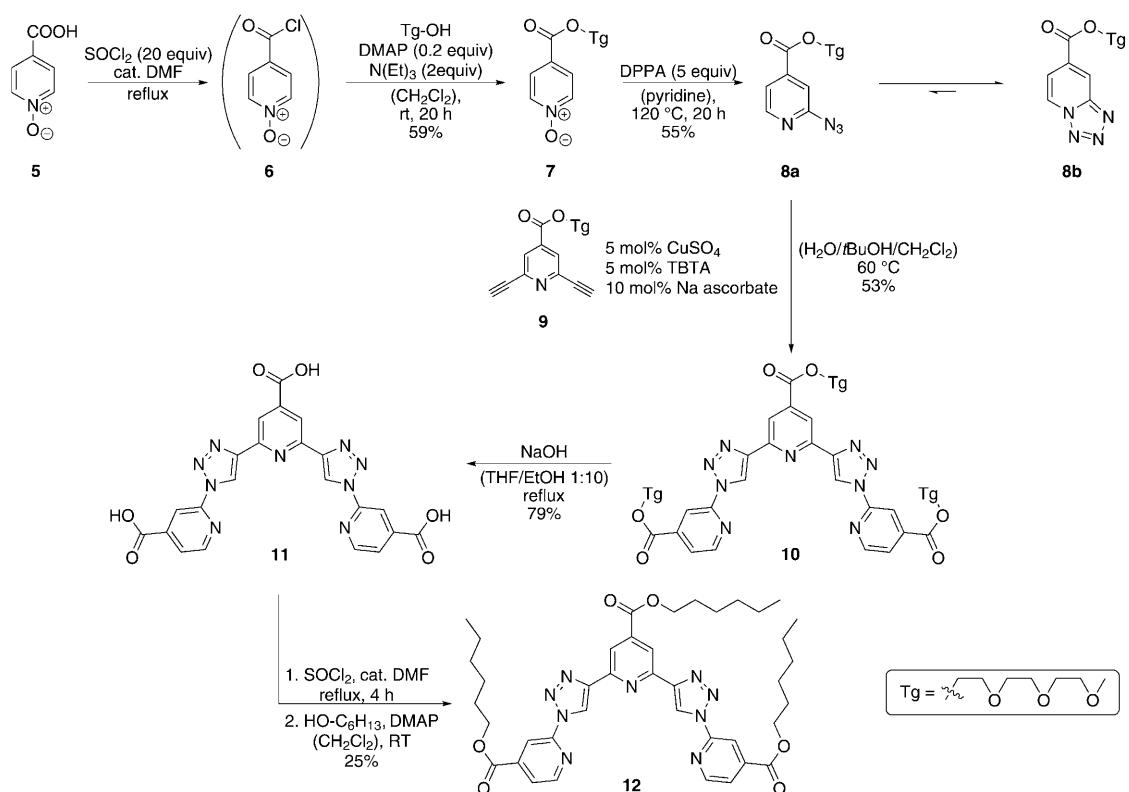


Figure 2. Single-crystal structure of compound **12** with the average bond lengths $\bar{d}_{C-C} = (1.463 \pm 0.045) \text{ \AA}$, and $\bar{d}_{C-N} = (1.435 \pm 0.015) \text{ \AA}$, and average dihedral angles $\bar{\vartheta} = (178.0 \pm 2.0)^\circ$, and $\bar{\phi} = (174.2 \pm 3.8)^\circ$ (average bond lengths and angles of the eight molecules contained in one unit cell).

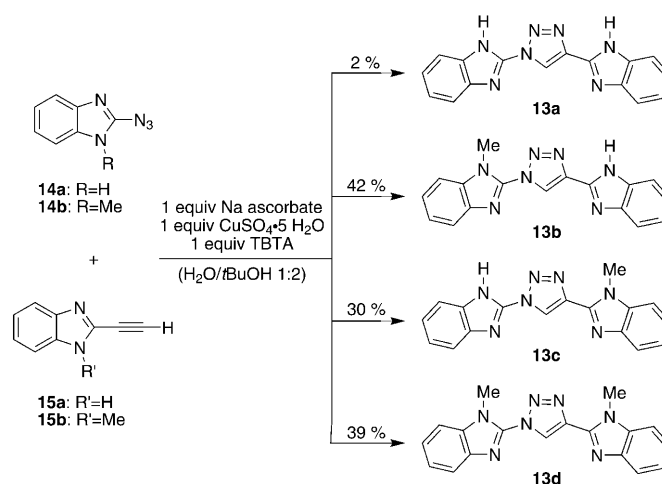
of the azide functionality failed. As a result, the rigid oligo/poly(pyridine-triazole)s—although most likely giving rise to a very stable helical structure—could not be accessed and therefore alternative building blocks, which connected the triazole moieties at their N(1) termini, were investigated.



Scheme 3. Synthesis of all-(pyridine-triazole) oligomer **12**.

Subsequently, our interest was focused on 2-(1,2,3-triazol-4-yl)benzimidazoles. In addition to its extended annelated backbone, the benzimidazole ring offers both remote donating and accepting interaction sites, that is, N(1) and lone pair N(3). The further increased outer bond angles of the five-membered ring should enable the tuning of the dihedral angles about the N(1)-triazolyl-2-benzimidazolyl bond and the C(4)-triazolyl-2-benzimidazolyl bond, respectively. To compare conformational preferences with the pyridine motif, the benzimidazole derivatives **14** and **15** were reacted by means of click chemistry to generate target compound **13**. To obtain additional information about the influence of electrostatic interactions between the N(2,3)-triazolyl and H(1)-benzimidazolyl atoms, N–H as well as N'–H were consecutively N-methylated to yield all four possible combinations, that is, **13a–d** (Scheme 4).

First assumptions of a preferred *anti-anti* conformation in solution were supported by extensive NOESY experiments of **13a–c** in [D₆]DMSO. As we did not attempt to observe a heteronuclear NOE between the triazole C(5) and the benzimidazole N(1) atoms in **13a–c** due to the low abundance of ¹⁵N, the actual conformation can only indirectly be inferred by the absence of a cross-peak between the triazole and benzimidazole protons (see Figures S17–S19 in the Supporting Information), thereby suggesting their large spatial separation and hence pointing to their relative *anti* relationship. Crystal structures of **13b** and **13d** (Figure 3), obtained by slowly evaporating the DMSO solvent at room temperature,



Scheme 4. Synthesis of benzimidazole-triazole-benzimidazole model compounds **13a–d**.

confirmed these findings as the *anti-anti* conformations could clearly be identified for these two compounds. The crystal structure of **13a**, unfortunately, shines no light on its conformation because the N(1) atoms in **13a** cannot clearly be assigned to either one side of the benzimidazole in the obtained data set. Note that in solution the imidazole N(1) atoms show tautomerism that could clearly be observed in the corresponding NOESY-spectrum (see Figure S17). Im-

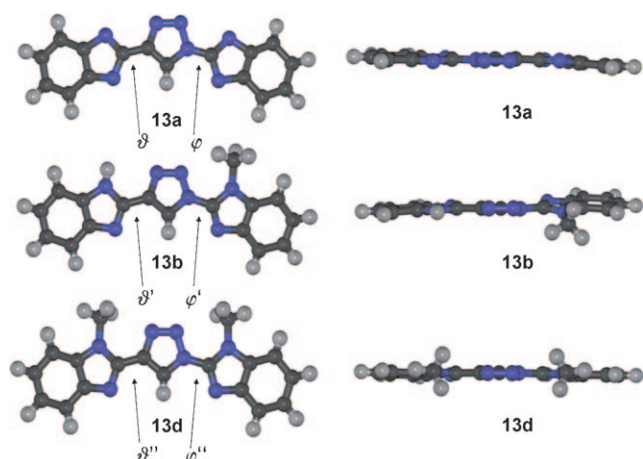


Figure 3. Molecular structures of benzimidazole-triazole-benzimidazole model compounds **13a,b,d**. Selected bond lengths [Å] and dihedral angles [°] in **13a** (averaged): $\bar{d}_{C-C} = (1.441 \pm 0.023)$, $\bar{d}_{C-N} = (1.388 \pm 0.023)$; $\vartheta = (176.6 \pm 0.1)$, $\phi = (174.8 \pm 3.0)$ (average bond lengths and angles of the two molecules contained in one unit cell); in **13b**: $d_{C-C} = 1.470$, $d_{C-N} = 1.418$; $\vartheta = 175.2$, $\phi = 160.9$; and in **13d**: $d_{C-N} = 1.436$, $d_{C-N} = 1.418$; $\vartheta = 175.4$, and $\phi = 177.7$.

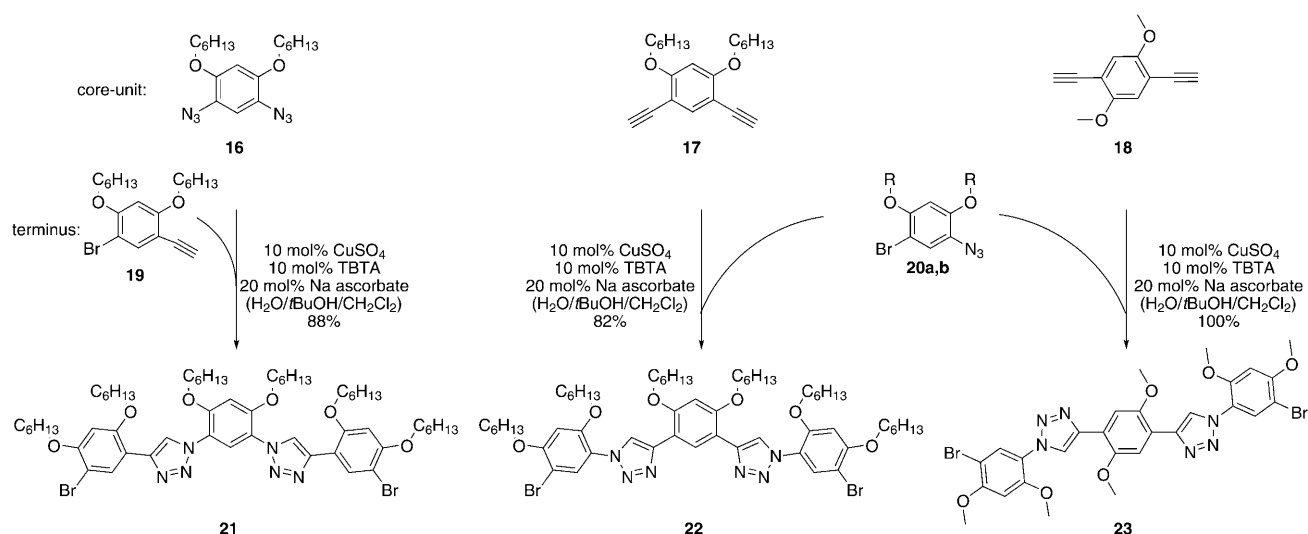
portantly, all three systems show a planar arrangement of the respective aromatic units (Figure 3, side views). Whereas **13a** and **13d** are completely planar, the benzimidazole moiety connected through the C–N bond of **13b** is twisted by 19.1°, which is probably induced by crystal packing.

Conformational constraints based on H···O interactions: An alternative conformationally restricting element, which is commonly used to bias the conformation of aromatic amides, is based on *ortho*-alkoxy substitution. The resulting interaction between neighboring hydrogen and O atoms leads to a wide variety of foldamer structures reported over the past years,^[19–21] however, they are solely restricted to

amide connectivities. To see whether a triazole-derived aromatic foldamer strand would gain additional stabilization by introducing *ortho*-alkoxy substituents, various alkylated resorcinol derivatives were linked by means of the click reaction. The required model compounds **21**, **22**, and **23** could be obtained in good and very good yields from the respective azide and ethynyl precursors **16–20** (Scheme 5; see also Figure S3 in the Supporting Information).

The connectivity in the *meta*-substituted, and therefore kinked, derivatives **21** and **22** is different as the first one is based on the diazide core **16**, whereas the latter one is formed from the diethynyl core **17**. Related compounds **21** and **22** display considerably different chemical shifts in the aromatic region of their NMR spectra (Figure 4, top). In particular, the strong chemical-shift difference of the central proton adjacent to the triazole moiety is remarkable, as the corresponding signal, located at $\delta = 9.29$ ppm (H_f) in **22**, experiences a significant upfield shift to $\delta = 8.06$ ppm (H_b) in **21**. This can be explained by the electron-donating mesomeric (+M) effect of both adjacent N(1)-triazole atoms in compound **21**, thus causing a shielding of the central phenyl proton relative to compound **22**.

The NOESY spectrum of **21** (Figure 4) shows only cross-peaks for the methylene protons to each other as well as to their adjacent *ortho*-phenylene protons H_a and H_c . No cross-peaks between the triazole protons H_T and their adjacent *ortho*-phenylene protons H_b and H_d , respectively, are observed. This finding supports the assumption that the *syn-syn* conformation is not adopted and hence suggests that the preferred *anti-anti* conformation, in which these protons are located at maximum distance, is populated. Also, in the NOESY spectrum of **22** (Figure 4), no cross-peaks between the triazole protons H_T and their neighboring *ortho*-phenylene protons H_f and H_h are observed, and again the only cross-peaks involve the methylene protons of the *n*-hexyl side chains. Therefore, compound **22** also seems to adopt an



Scheme 5. Synthesis of resorcinol-triazole-resorcinol model compounds **21–23** with R = C₆H₁₃ (**21**, **22**) and CH₃ (**23**), shown in their preferred *anti-anti* conformations.

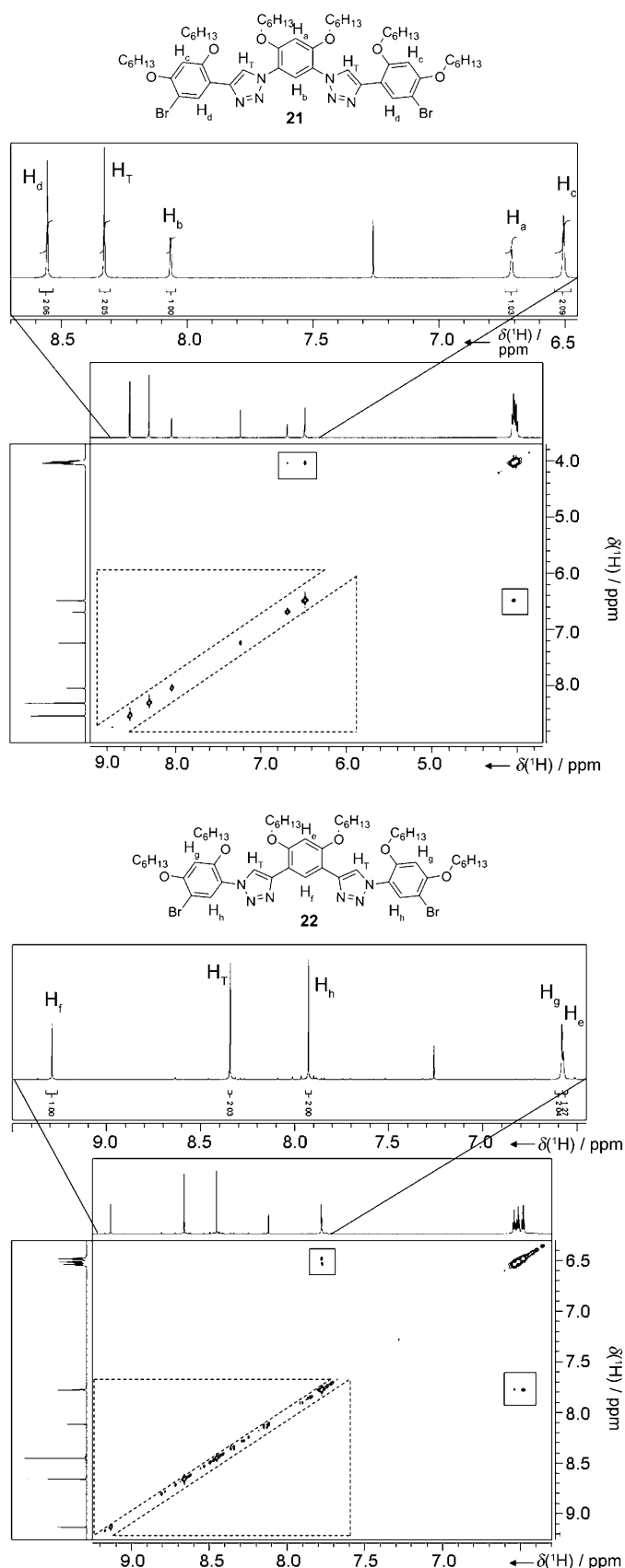


Figure 4. NOESY spectra of **21** (top) and **22** (bottom) including ^1H NMR spectra. Apparent cross-peaks for methylene protons to adjacent *ortho*-phenylene protons H_d as well as H_c are shown in black boxes. Expected regions with absent cross-peaks between the triazole proton and the adjacent *ortho*-phenylene protons H_T and H_b and H_d (for **21**) and H_i and H_j (for **22**), respectively, which confirm the preferred *anti-anti* conformation, are marked with dashed lines.

anti-anti conformation in solution. Single crystals of **21** could be obtained by slowly evaporating the NMR spectroscopic solvent CDCl_3 at room temperature, and the molecular structure reveals the expected *anti-anti* conformation (Figure S5 in the Supporting Information). However, the quality of the obtained structural data was limited with final R indices above 10% ($wR = 14\%$), probably due to the poor packing of the *n*-hexyl chains. Unfortunately, no single crystals could be obtained in the case of compound **22**.

When the *meta*-substituted aromatic core unit is displaced by the *para*-substituted diacetylene **18**, the resulting oligomer structure was not kinked, but rather linear. In contrast to compounds **21** and **22**, the cross peaks between the triazole proton H_T and the adjacent *ortho*-phenylene proton H_k in the NOESY spectrum of **23** (see Figure S22 in the Supporting Information) are not completely absent. The intensity of these cross-peaks, however, is negligible (comparable signal-to-noise ratio to the t_1 streaks). Thus we believe that **23** also adopts the expected *anti* conformation. In this case, methyl groups were introduced instead of hexyl chains to grow high-quality crystals of **23**. Structural analysis shows that the molecule adopts the *anti-anti* conformation (Figure 5). More importantly, the structure exhibits nearly perfect planarity (dihedral angle of 0.2°) in the core region

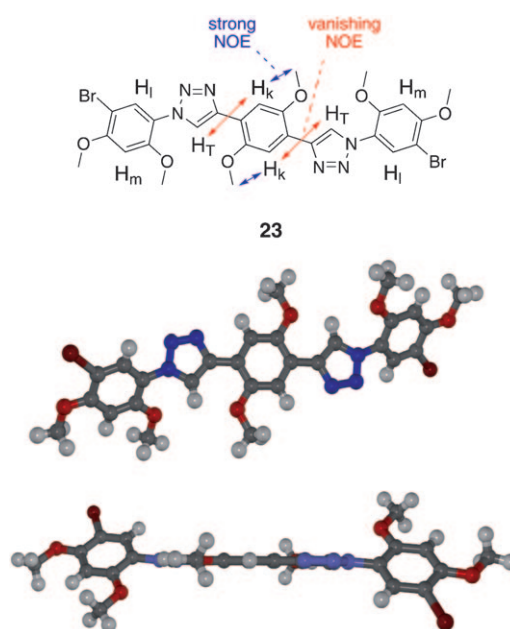


Figure 5. Single-crystal structure of compound **23** with C_i symmetry with selected bond lengths $d_{\text{C-C}} = 1.531 \text{ \AA}$ and $d_{\text{C-N}} = 1.530 \text{ \AA}$ and selected dihedral angles $\vartheta = 0.2^\circ$ and $\phi = 42.7^\circ$ (middle: top view; bottom: side view).

that involves a triazol-4-yl connection, that is, along a C–C bond, whereas the terminal resorcinol units are significantly twisted by 42.7° about the triazol-1-yl linkage, that is, the C–N bond. This points to the importance of connectivity in this system. Whereas the attachment through the C(4) position of the triazole as in **23** gives rise to the desired highly planar *anti* arrangement, the alternative attachment through the N(1) position of the triazole leads to a significantly twisted *anti* conformation. This distortion is most likely caused by steric repulsion, which furthermore also leads to an elongation of the connecting N(1)–C bond ($d_{\text{C-N}} = 1.530 \text{ \AA}$) as compared to the parent unsubstituted 1-phenyl-1,2,3-triazoles ($d_{\text{C-N}} = 1.429 \text{ \AA}$ as well as 1.443 \AA).^[21,22]

The maximum benefit of these structural motifs would be gained when different building blocks, which possess their distinct conformational properties, could be combined in a construction kit principle and any desired foldamer shape could be afforded consequently. For this purpose, mixed systems that comprised a central BTP unit with terminal *ortho*-alkoxy-substituted phenyl moieties were synthesized. Two pyridine cores (Figure 6) were introduced to yield two

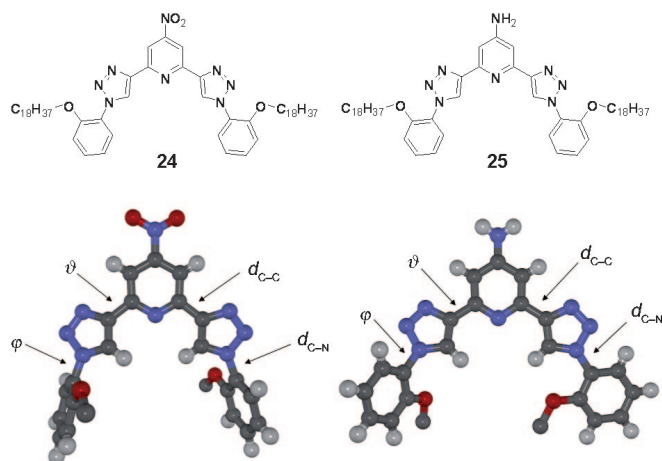


Figure 6. Structures and conformational preferences of mixed systems **24** and **25** for the *anti-anti* conformation in the solid that bears the structure-directing pyridine–triazole connection as well as the *ortho*-alkoxy-phenylene connection with selected bond lengths [\AA] and dihedral angles [$^\circ$] of **24**: $d_{\text{C-C}} = 1.466$ and $d_{\text{C-N}} = 1.427$ and $\vartheta = 10.9$ and $\phi = 55.2$; **25**: $d_{\text{C-C}} = 1.471$ and $d_{\text{C-N}} = 1.432$ and $\vartheta = 6.4$ and $\phi = 31.8$.

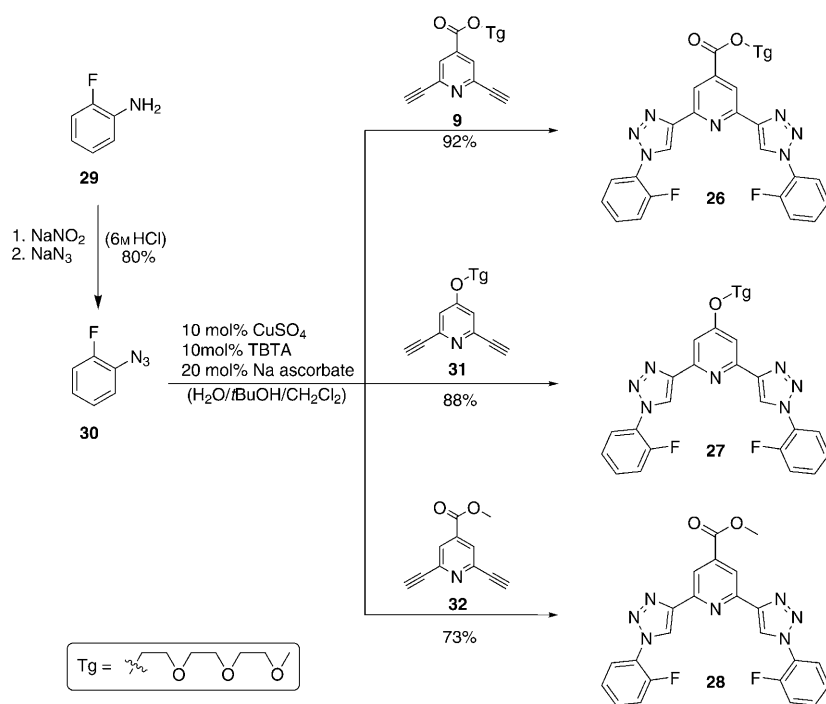
model compounds with different substitution, as electron-withdrawing nitro (**24**) and electron-donating amino functionality (**25**), in the 4-position of the pyridine, yet both bearing an *ortho*-alkoxy substituent. These compounds could be easily synthesized in very good yields by adapting a convergent procedure. To show that the structural considerations proven for the structures above are also valid for mixed structures, both compounds were studied in solution by NOESY and in the solid state by crystal-structure analysis, respectively. As expected, the conformation in solution adopts the preferred *anti-anti* orientation as neither a cross-peak between the triazole proton with the C(3,5) proton of

the pyridine nor with the protons of the phenylene can be observed (Figure S23 and S24 in the Supporting Information). The structure analyses of both crystals, shown in Figure 6, also reveals the backbone that adopts the preferred *anti* conformation not only at the pyridine-bridged triazole connectivity, but also at the *ortho*-alkoxy-substituted phenyl-triazole connection as well. Whereas the pyridine-triazole-connectivity through C–C linkage shows nearly planar conformation, the *ortho*-alkoxy-substituted phenylenes show a perceivable twist for the C–N linkage, as was already observed in compounds **21** and **23**. When the dihedral angles are taken into account, it is noteworthy that **24** shows somewhat comparable values of $\vartheta = 10.9^\circ$ and $\phi = 55.2^\circ$ to compound **25** with $\vartheta = 6.4^\circ$ and $\phi = 31.8^\circ$, thereby indicating that not only the choice of the structure-directing heteroatom directly influences the conformational design of the resulting oligomer and polymer vice versa, but also the steric demand of *ortho*-alkoxy substituent. On the contrary, the electronic effects of the C(4) substituents of the pyridine seem to be negligible due to similar torsions of the withdrawing nitro and donating amine compound.

Conformational constraints based on H...F interactions:

With the knowledge that halogen substituents serve as potential hydrogen-bond acceptors as well,^[23] we further examined the structure-inducing influence of *ortho*-substituted fluorobenzene on the triazole moiety to expand the variety of structure-inducing substituents in our toolbox. Fluorine as a strong proton acceptor asserted itself in that field,^[24] although its application has been quite limited up to now. Therefore, we decided to prepare compounds **26** and **27** (Scheme 6), which again were functionalized with electron-withdrawing and electron-donating in the C(4) position of the pyridine to investigate their structural influences in solution. The *ortho*-fluorophenyl azide **30** was reacted with the three different bis(ethynyl)pyridines **9**, **31**, and **32** to afford click products **26**, **27**, and **28**, respectively. Whereas the tri-glyme side chain in **26** and **27** provide solubility for conformational characterization in solution, the methyl derivative **28** was prepared to obtain single crystals suitable for X-ray crystallography.

Electron-donating and -accepting properties of the obtained click products can be observed as expected by the significant difference of the protons of the pyridine on C-(3,5) upfield-shifted from $\delta = 8.78$ ppm in **26** to $\delta = 7.79$ ppm in **27**, yet are barely reflected by the triazole shifts from $\delta = 8.75$ ppm (**26**) to $\delta = 8.70$ ppm (**27**). Indications for the anticipated *anti-anti* conformation can already be extracted from 1D proton spectra: the triazole protons are split by a “through-space” $^5J(\text{H}, ^{19}\text{F})$ scalar coupling of 2.7 Hz for both **26** and **27**.^[25] Additional evidence is provided from homo- and heteronuclear NOE experiments since cross-peaks between the triazole proton and the *ortho*-phenyl proton are again absent. As a big advantage of these systems, a spatial proximity between the fluoro atoms and triazole protons could directly be detected qualitatively in ^1H - ^{19}F 2D heteronuclear NOESY (HOESY) experiments as evidenced by



Scheme 6. Synthesis of fluoro-substituted click compounds **26–28**.

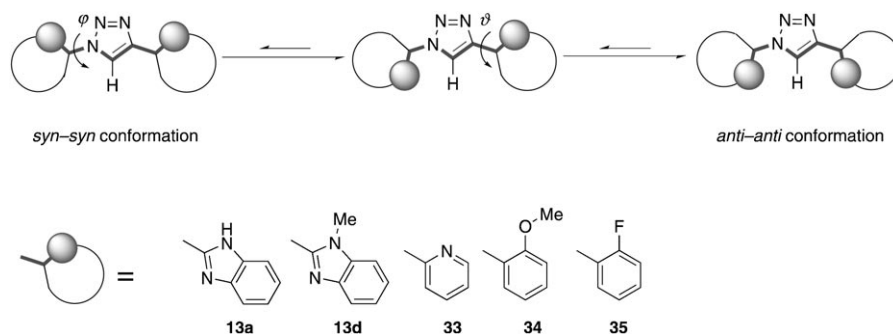
cross-peaks between the triazole proton and the fluoro substituent of the benzene ring (Figure 7).

These findings could analogously be supported by crystal-structure analyses of **28**, which was successfully crystallized twice by slow evaporation of THF on the one hand and CDCl₃ on the other (Figure 8). Again, in this type of model compound, the BTP core shows a well-established horse-shoelike structure. Interestingly, the choice of solvent influenced the conformational situation of the molecule in lattice around the N(3) connection of the triazoles and the C(1) connection of the phenylenes. Whereas crystals grown in THF showed a twist of both *ortho*-fluoro-substituted phenyl rings of 23.7 and 32.1° out of the molecular plane, crystals grown from CDCl₃ reveal this twist on only one side, which is probably induced by cocrystallized solvent molecules in the crystal package. Nevertheless, both structures adopt the preferred *anti-anti* conformation on both the C–N as well as the C–C connectivity, as was expected by preliminary considerations.

Computational studies: To evaluate and rationalize our experimental findings, first DFT calculations were carried out by computing the rotational barrier between the *syn-syn* and *anti-anti* conformations about the triazole-phenyl linkage in the gas phase. Theoretical considerations reveal three major

forces that contribute to the potential energy diagram (Figure 9) for the triazole-phenyl rotamers. On the one hand, repulsive forces increase (dotted line in Figure 9), as the triazole proton and the *ortho*-phenyl proton on one side of the molecule as well as the phenyl *ortho* substituent and the lone pair of the triazole N(2) atom on the other side experience spatial proximity. This steric repulsion will be reduced by turning the dihedral angle in the opposite direction, therefore placing the triazole and *ortho*-phenyl protons in an *anti* relationship. On the other hand, while these steric repulsive forces are being reduced, additional attractive forces arise (solid line in Figure 9) to further reduce the potential energy in the *anti* conformation.

This effect originates from the electrostatic attraction (hydrogen bond) between the triazole nitrogen lone pairs and the *ortho*-phenyl proton as well as the *ortho*-heteroatom and the triazole proton in the *anti* conformation. Last but not least, forcing the phenyl rings away from coplanarity results in a loss of π conjugation (dashed line in Figure 9), thereby leading to an increase of potential energy, which reaches its maximum at the perpendicular orientation of two adjacent aromatic systems, that is, the transition state for rotation. For representative and comparable calculations, appropriate model compounds were chosen that consisted of a central triazole moiety connected on both its N(1) and C(4) positions to *ortho*-substituted phenyl rings with the investigated heteroatom functionalities attached, which are essential for rotational restriction (Scheme 7). After geometry optimization using the B3LYP density functional with the TZVP basis set, the backbone coordinates were restricted and only



Scheme 7. Model compounds **13a**, **13d**, **33**, **34**, and **35** established for computational studies.

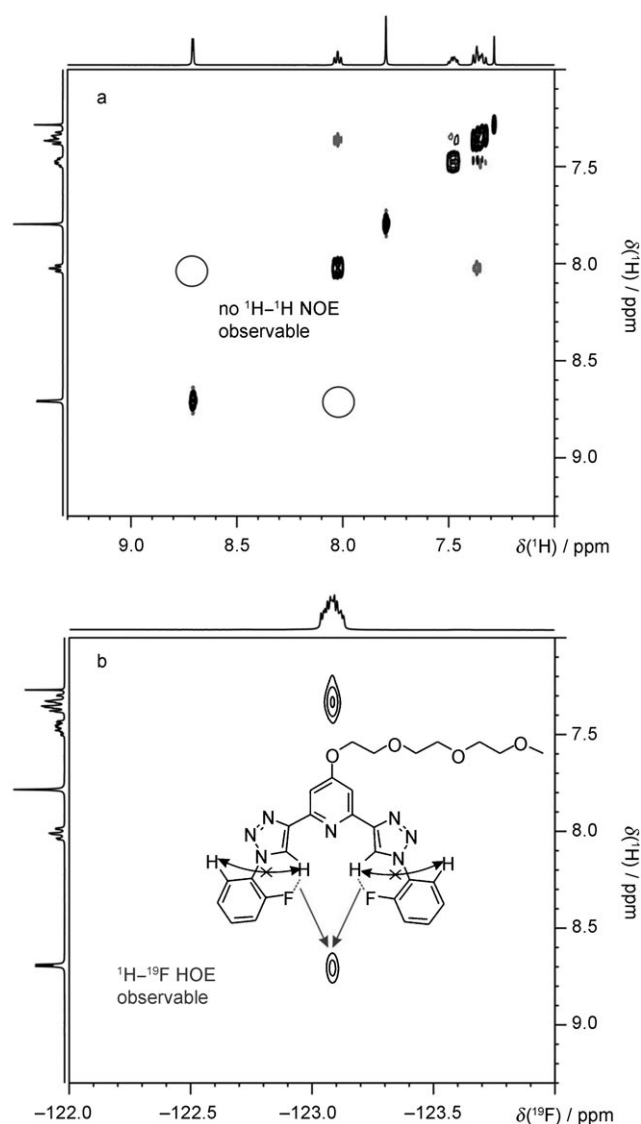


Figure 7. a) Partial ^1H - ^1H NOESY (500 MHz, 1 s mixing time) and b) ^1H - ^{19}F HOESY spectra (300 MHz, 200 ms mixing time; see the Supporting Information) of compound **27**, showing the absence of a ^1H - ^1H NOE between the triazole proton and the *ortho*-proton of the terminal phenyl moiety and the presence of a ^1H - ^{19}F HOE between the triazole proton and the *ortho*-fluorine atoms. For compound **26**, essentially identical results were obtained (data not shown).

the phenyl rings were subsequently twisted by incremental steps of 10° . Then, absolute energies were calculated and plotted against the corresponding dihedral angles ϕ and ϑ , which related to rotation about the N(1)-C and C(4)-C bonds, respectively. This rather crude but less intense scanning procedure was adapted to all five experimentally investigated motifs. The obtained results (Table 1) give insights into the minimum conformations ($\vartheta_{\text{opt}}/\phi_{\text{opt}}$), their relative thermodynamic stabilities (ΔH) as compared to an alternative conformation (local minimum), and the barrier of rotation (ΔH^\ddagger).

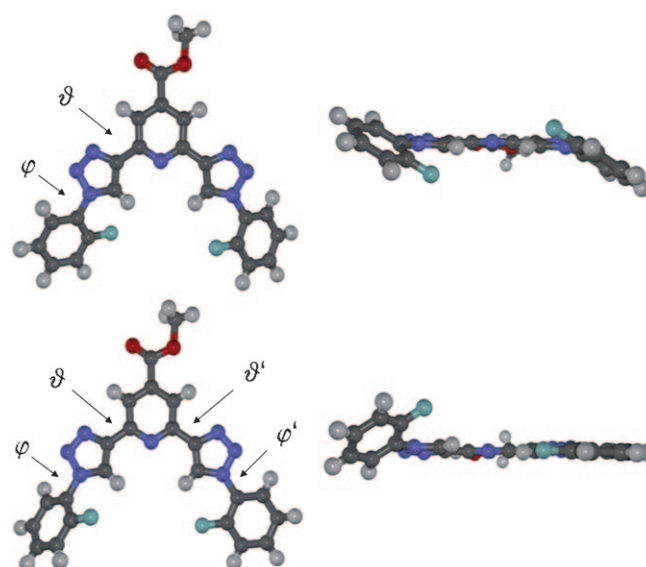


Figure 8. Crystal structures of **28** are illustrated as on-top-view (left) and in-plane-view (right) with selected bond lengths [\AA] and dihedral angles [$^\circ$] crystallized from THF (top): $d_{\text{C-C}}(\vartheta)=1.301$, $d_{\text{C-N}}(\phi)=1.224$ and $\vartheta=4.1$, $\phi=32.1$; and crystallized from CDCl_3 (bottom): $d_{\text{C-C}}(\vartheta)=1.638$, $d_{\text{C-C}}(\vartheta')=1.995$, $d_{\text{C-N}}(\phi)=1.696$, $d_{\text{C-N}}(\phi')=1.372$ and $\vartheta=2.6$, $\vartheta'=5.0$, $\phi=41.2$ and $\phi'=2.4$.

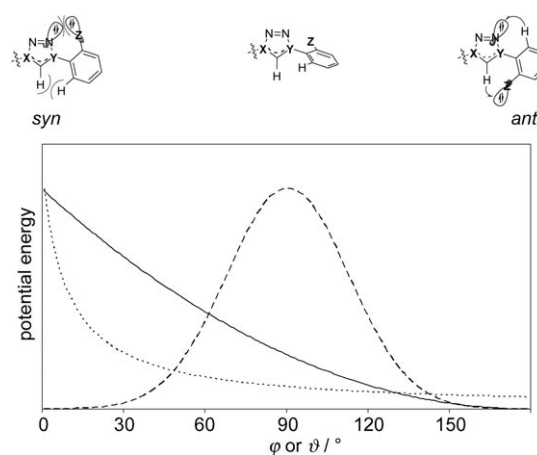

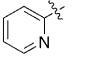
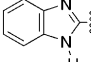
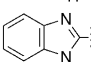
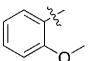
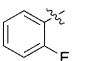


Figure 9. Expected energetic contributions that result from repulsive (dotted) and attractive interactions (solid) as well as the loss of aromaticity (dashed). Z denotes the *ortho*-heteroatom substituent, X and Y are either N(1) (related to ϕ) or C(4) (related to ϑ) of the triazole moiety and vice versa.

Former DFT calculations on a 4-(2-pyridyl)-1,2,3-triazole model system predicted a conformational preference along the C(4)-C connection for the *anti* conformation of $6.4 \text{ kcal mol}^{-1}$ over the *syn* conformer in the gas phase,^[12] which was slightly larger than the comparable conformational preference of 2,2'-bipyridines ($5.9 \text{ kcal mol}^{-1}$).^[26] Unfortunately, these calculations provide no insight into the energetics at the N(1)-C connection. Therefore, the pyridine motif was investigated again and relevant parameters calculated for both connectivities—that is, C(4)-C and N(1)-C—at this time. Geometry optimization provided a completely

Table 1. Rotational parameters calculated by means of DFT (B3LYP, TZVP).



	ϕ_{opt} [°] ^[a]	ΔH [kcal mol ⁻¹] ^[b]	ϕ_{alt} [°] ^[c]	ΔH^{\ddagger} [kcal mol ⁻¹] ^[d]	ϕ^{\ddagger} [°] ^[e]	$d(\text{H}-\text{X})$ [Å] ^[f]	ϑ_{opt} [°] ^[a]	ΔH [kcal mol ⁻¹] ^[b]	ϑ_{alt} [°] ^[c]	ΔH^{\ddagger} [kcal mol ⁻¹] ^[d]	ϑ^{\ddagger} [°] ^[e]	$d(\text{H}-\text{X})$ [Å] ^[f]
	0	6.1	140	6.7	100	2.6	0	6.8	150	8.1	90	2.9
	0	o.o.m.	o.o.m.	11.0	180	2.8	0	7.6	160	8.9	100	3.1
	0	o.o.m.	o.o.m.	17.3	180	2.6	0	o.o.m.	o.o.m.	16.0	180	2.9
	42	7.4	42	9.7	180	2.5	3	5.0	130	5.3	100	2.4
	34	6.4	110	2.0	100	2.4	0	4.7	130	5.4	100	2.4

[a] Rotational angle in fully optimized geometry of most stable conformer. [b] Stabilization relative to alternative conformation (if existing, o.o.m. = only one minimum). [c] Rotational angle in local minimum conformation. [d] Rotational barrier to alternative minimum or for full rotation. [e] Torsion angle of conformation displaying the highest rotational barrier. [f] Distance between the nuclei of the triazole HC(5) and the respective adjacent heteroatom X.

planar—that is, flat—structure with both torsion angles ϕ and ϑ equal to 0°. The barrier for rotation ΔG^{\ddagger} was calculated to be 7.2 kcal mol⁻¹ for the twist around the C–N bond, whereas the *syn* conformation at the C–C linkage was determined to be 8.1 kcal mol⁻¹ higher in energy than the *anti* conformation. These values for both connectivities are larger than Lehn and co-workers' 2,2'-bipyridine motif.^[26] Astonishingly high rotational barriers were calculated for the benzimidazole motif. Due to the increased outer bond angles associated with the five-membered triazole ring, the dihedral angles about the N(1)–2-benzimidazolyl and the C(4)–2-benzimidazolyl bonds should reduce the steric repulsion between adjacent substituents on both heteroaryl moieties. Consequently, compound **13a** and **13d** were calculated to be planar in their geometry-optimized states. The rotational barriers of **13a** were calculated to be 11.0 kcal mol⁻¹ for the N–C connection related to ϕ and 8.9 kcal mol⁻¹ for the C–C connection related to ϑ , which is in agreement with the shorter N–C bond as evidenced by X-ray crystal-structure analysis. Interestingly, introduction of the N-methyl substituents in the benzimidazole moieties does not lead to a destabilization of the *anti-anti* conformation, and instead the N-methylated derivative **13d** displays even higher rotational barriers that amount to 17.3 and 16.0 kcal mol⁻¹, respectively. This effect seems to originate from the stabilization of the *anti-anti* conformation due to attractive electrostatic interactions between two methyl protons each and the neighboring N(2) and N(3) atoms relative to the significant destabilization of the *syn-syn* conformation by enhanced steric repulsion of the C(5)–H and both adjacent methyl groups. Compared to the BTP motif, it should be emphasized that the benzimidazole as the backbone entity shows an extraordinarily strong stabilization of the *anti-anti* con-

formers for both compounds. These results nicely illustrate that the linkage of two five-membered heteroaromatic rings is suitable to achieve flat, coplanar geometries due to the reduction of steric repulsion between adjacent substituents. Analogously to **13**, the optimized geometry as well as the rotational barriers were calculated for 1,4-bis(2-methoxyphenyl)-1*H*-1,2,3-triazole **34** as the model compound for alkoxy-substituted molecules. The minimum structure displayed a significant distortion about the N(1)–C bond that resulted in a dihedral angle ϕ of 42°, whereas the system remained essentially coplanar at the C(4)–C connection ($\vartheta = 3^\circ$). It should be noted that geometry optimization nicely reproduces the structural data derived experimentally from single-crystal-X-ray diffraction ($\phi = 42.7^\circ$, $\vartheta = 0.2^\circ$). A potential explanation for the deviation from coplanarity in the case of the N(1)–C connection involves a stabilizing HOMO–LUMO interaction, which can occur in the twisted geometry only (Figure S16 in the Supporting Information). Neglecting the presence of a shallow minimum in the case of the C(4)–C connection (Figure S14), the global minima (*anti* conformers) are slightly more stable in the case of the N(1)–C connection (9.4 kcal mol⁻¹) as compared to the C(4)–C connection (8.2 kcal mol⁻¹) with regard to their *syn* counterparts (dihedral angles ϕ and $\vartheta = 180^\circ$). As compared to the benzimidazole motif, the rotational barriers in **34** amount to only one half; however, they are sufficiently high enough to enable the use of *ortho*-alkoxy substitution as a conformation-restricting motif. Similar results were obtained for the calculation of the fluorine analogue **35**. *Ortho* substitution by fluorine also causes a phenyl twist of 34° for the N(1)–C bond that relates to ϕ , whereas the C(4)–C connection was repeatedly predicted to be coplanar ($\vartheta = 0^\circ$). The relative stability of the *anti* conformers with regard to the

syn conformations amounts to $6.4 \text{ kcal mol}^{-1}$ in both cases, that is, for torsion angles ϕ as well as ϑ . When comparing these results with our H...N and H...O motifs, these values represent the lowest rotational barriers yet they are still higher than the barrier calculated for Lehn and co-workers' 2,2'-bipyridine motif,^[26] and therefore also an *ortho*-fluorine substitution should be able to induce the desired conformational preferences. Taking into account all the calculated relative stabilities of the various conformers, useful energetic considerations for foldamer design emerge (Figure 10). In

Conclusion

Conformationally preorganized motifs for triazole-based foldamers based on adjacent heteroatom substituents have experimentally and theoretically been investigated. Various suitable model compounds were prepared and investigated with regard to their preferred conformations in the gas phase, in solution, and in the solid state by employing DFT calculations, NMR spectroscopic experiments, and X-ray crystallography, respectively. The results show that the introduced N-, O-, and F-substituents induce rotational constraints around the single bonds attached to the 1- and 4-positions of the 1,2,3-triazole and hence the investigated motifs should lead to well-defined conformational preferences in higher oligomers and polymers, that is, "clickamers." On the basis of the thus-obtained general understanding of the conformational behavior of the individual connection motifs, heterostructures composed of different motifs could be prepared without affecting their distinct conformational characteristics. These studies support the general concept of triazole-based foldamers and, for the first time, provide rather detailed information useful for designing new "clickamer" backbones.

By using this toolbox and rationally introducing the right heteroatom substituents in the correct positions, folded conformations with enhanced stability can be created while maintaining synthetic accessibility by means of click chemistry.

Currently, ongoing work in our laboratories is focused on clickamers derived from connecting aromatic ethers to obtain elongated helical or linear tape structures and the incorporation of functional groups to induce self-assembly and to provide response to external stimuli, in particular light.^[28] In the future, the concept of the preparation of new foldamer backbones by means of click chemistry should enable the design of a wide variety of highly sophisticated functional yet nonbiological macromolecules by combining defined secondary (and higher structures) with the facile incorporation of any desired functional entity. In addition to specific efforts, this endeavor will greatly benefit from stronger theoretical involvements including the computation of larger structures and their dynamics in solution.^[29]

Experimental Section

Experimental details can be found in the Supporting Information. CCDC-759338 (**12**), 759332 (**13a**), 759331 (**13b**), 759330 (**13c**) and 759335 (**23**) contain the supplementary crystallographic data for this paper. These data can be obtained free of charge from The Cambridge Crystallographic Data Centre via www.ccdc.cam.ac.uk/data_request/cif.

Acknowledgements

The authors thank Dr. B. Ziemer (HU Berlin) for carrying out the single-crystal X-ray structure analyses and Merck KGaA (Darmstadt)—es-

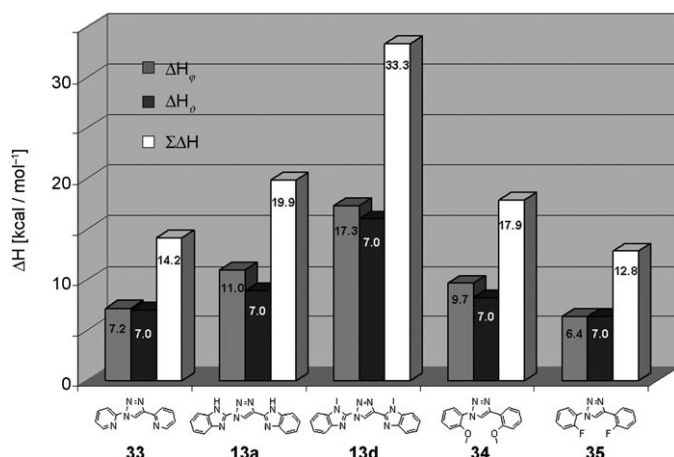


Figure 10. Stabilization energies ΔH for the *anti*-conformation compared to the *syn*-conformation by rotating the dihedral angles ϕ (C–N bond) and ϑ (C–C bond) from 0 to 180°.

each clickamer motif, there are two connectivities associated with a preferred and a nonpreferred conformation, that is, *anti* and *syn* conformations, respectively. As the triazole moiety intrinsically always provides two connections, one has to consider the superposition of these partial conformational equilibria, that is, four different conformations (*anti-anti* vs. *anti-syn* vs. *syn-anti* vs. *syn-syn*).

To guide the design of global helical structures with enhanced stability, which geometrically arises from the *anti-anti* conformation, its stabilization relative to all other possible conformations is the most important parameter to optimize; and clearly, from the data provided in Figure 10, privileged structure types can be derived. The basis of these privileged kinked or zigzag flat structures is the balancing of stabilizing electrostatic (i.e., hydrogen-bonding) interactions with the counteracting destabilizing steric repulsion that arises from the close proximity of the adjacent substituents/atoms. Note that hydrogen bonding occurs most likely through space (distances see Table 1), although alternatively through-bond interactions are also conceivable. Clearly more elaborate computational work will be necessary to unambiguously understand the basis for the observed conformational preferences in the systems investigated herein.^[27]

pecially M. Schwarzkopf-Hofmann—for helpful discussions and granting access to the DPX 300 NMR spectrometer for ^1H - ^{19}F HOESY measurements. Generous support by the German Research Foundation (DFG through the SFB 765, Emmy Noether programme TH1115/3-1 to C.M.T.) and the Fonds der Chemischen Industrie is gratefully acknowledged. Wacker Chemie AG, BASF AG, Bayer Industry Services, and Sasol Germany are thanked for generous donations of chemicals.

- [1] Special Issue: Supramolecular Chemistry and Self-Assembly, J.-M. Lehn, *Science* **2002**, *295*, 2400–2403.
- [2] For representative reviews, see: a) F. Bates, *Science* **1991**, *251*, 898–905; b) S. Förster, M. Antonietti, *Adv. Mater.* **1998**, *10*, 195–217; c) M. Lee, B.-K. Cho, W.-C. Zin, *Chem. Rev.* **2001**, *101*, 3869–3892; d) S. Jain, F. Bates, *Science* **2003**, *300*, 460–464.
- [3] For two instructive reviews on supramolecular polymers, see: a) L. Brunsveld, B. J. B. Folmer, E. W. Meijer, R. P. Sijbesma, *Chem. Rev.* **2001**, *101*, 4071–4097; b) T. F. A. De Greef, M. M. J. Smulders, M. Wolfs, A. P. H. J. Schenning, R. P. Sijbesma, E. W. Meijer, *Chem. Rev.* **2009**, *109*, 5687–5754.
- [4] a) G. R. Newkome, C. N. Moorefield, F. Vögtle, *Dendrimers and Dendrons. Concepts Syntheses Applications*, Wiley-VCH, Weinheim, **2001**; b) J. M. J. Fréchet, D. A. Tomalia, *Dendrimers and other Dendritic Polymers* (Wiley Series in Polymer Science), West Sussex, **2002**.
- [5] a) S. H. Gellman, *Acc. Chem. Res.* **1998**, *31*, 173–180; b) D. J. Hill, M. J. Mio, R. B. Prince, T. S. Hughes, J. S. Moore, *Chem. Rev.* **2001**, *101*, 3893–4011; c) *Foldamers: Structure Properties and Applications* (Eds.: Hecht, S.; Huc, I.), Wiley-VCH, Weinheim, **2007**.
- [6] For example, see: a) S. Hecht, *Materials Today* **2005**, *8*, 48–55; b) C. J. Hawker, K. L. Wooley, *Science* **2005**, *309*, 1200–1205.
- [7] The enormous helix stability of a pyridine dicarboxamide foldamer is exemplified as it can only be denatured in strong acids: a) C. Dolain, V. Maurizot, I. Huc, *Angew. Chem. Int. Ed.* **2003**, *42*, 2738–2740 and not in dimethyl sulfoxide at 120 °C; b) N. Delsuc, T. Kawamura, J. Lefeuvre, A. Shundo, H. Ihara, M. Takafuji, I. Huc, *ChemPhysChem* **2008**, *9*, 1882–1890.
- [8] For reviews, see: a) I. Huc, *Eur. J. Org. Chem.* **2004**, 17–29; b) Z.-T. Li, J.-L. Hou, C. Li, H.-P. Yi, *Chem. Asian J.* **2006**, *1*, 766–778; c) I. Huc, L. Cuccia in *Foldamers: Structure Properties and Applications* (Eds.: S. Hecht, I. Huc), Wiley-VCH, Weinheim, **2007**, pp. 3–33.
- [9] For solvophobic effects in foldamers, see: Y. Zhao, J. S. Moore in *Foldamers: Structure Properties and Applications* (Eds.: S. Hecht, I. Huc), Wiley-VCH, Weinheim, **2007**, pp. 75–108.
- [10] A notable exception is based on heteroaryl oligomers with incorporated *anti*-2,2'-bipyridyl linkages, historically developed first by Lehn and co-workers: J.-M. Lehn, A. Rigault, J. Siegel, *Proc. Natl. Acad. Sci. USA* **1987**, *84*, 2565–2569; G. S. Hanan, J.-M. Lehn, N. Kyritsakas, J. Fischer, *J. Chem. Soc. Chem. Commun.* **1995**, 765–766; A. R. Stefankiewicz, M. Walesa, P. Jankowski, A. Ciesielski, V. Patroniak, M. Kubicki, Z. Hnatejko, J.-M. Harrowfield, J.-M. Lehn, *Eur. J. Inorg. Chem.* **2008**, 2910–2920; M. Walesa, P. Jankowski, A. Ciesielski, V. Patroniak, M. Kubicki, Z. Hnatejko, J.-M. Harrowfield, J.-M. Lehn, *Eur. J. Inorg. Chem.* **2008**, 2910–2920.
- [11] For a review, see: Y. L. Angell, K. Burgess, *Chem. Soc. Rev.* **2007**, *36*, 1674–1689.
- [12] R. M. Meudtner, M. Ostermeier, R. Goddard, C. Limberg, S. Hecht, *Chem. Eur. J.* **2007**, *13*, 9834–9840.
- [13] For related approaches to pyridine–triazole oligomers by other groups, see: a) Y. Li, M. Pink, J. A. Karty, A. H. Flood, *J. Am. Chem. Soc.* **2008**, *130*, 17293–17295. For related approaches to phenylene-triazole oligomers, see: b) Y. Li, A. H. Flood, *Angew. Chem.* **2008**, *120*, 2689–2692; *Angew. Chem. Int. Ed.* **2008**, *47*, 2649–2652; c) H. Juwarker, J. M. Lenhardt, D. M. Pham, S. L. Craig, *Angew. Chem.* **2008**, *120*, 3800–3803; *Angew. Chem. Int. Ed.* **2008**, *47*, 3740–3743; d) Y. Li, A. H. Flood, *J. Am. Chem. Soc.* **2008**, *130*, 12111–12122; e) H. Juwarker, J. M. Lenhardt, J. C. Castillo, E. Zhao, S. Krishnamurthy, R. M. Jamiolkowski, K.-H. Kim, S. L. Craig, *J. Org. Chem.* **2009**, *74*, 8924–8934; f) Y. Wang, F. Li, Y. Han, F. Wang, H. Jiang, *Chem. Eur. J.* **2009**, *15*, 9424–9433; g) S. Lee, Y. Hua, H. Park, A. H. Flood, *Org. Lett.* **2010**, *12*, 2100–2102. An instructive review is given in: h) Y. Hua, A. H. Flood, *Chem. Soc. Rev.* **2010**, *39*, 1262–1271.
- [14] R. M. Meudtner, S. Hecht, *Angew. Chem.* **2008**, *120*, 5004–5008; *Angew. Chem. Int. Ed.* **2008**, *47*, 4926–4930.
- [15] M. Ostermeier, M.-A. Berlin, R. Meudtner, S. Demeshko, F. Meyer, C. Limberg, S. Hecht, *Chem. Eur. J.* **2010**, *16*, 10202–10213.
- [16] R. M. Meudtner, S. Hecht, *Macromol. Rapid Commun.* **2008**, *29*, 347–351.
- [17] L. Piot, R. M. Meudtner, T. El Malah, S. Hecht, P. Samori, *Chem. Eur. J.* **2009**, *15*, 4788–4792.
- [18] For a review on N-heteroaromatic azide–triazole tautomerization, see: a) M. Tisler, *Synthesis* **1973**, 123–136. Two recent examples include: b) B. Chattopadhyay, C. I. Rivera Vera, S. Chuprakov, V. Gevorgian, *Org. Lett.* **2010**, *12*, 2166–2169; c) M. K. Lakshman, M. K. Singh, D. Parrish, R. Balachandran, B. W. Day, *J. Org. Chem.* **2010**, *75*, 2461–2473.
- [19] Original work by the Huc/Lehn group: a) V. Berl, I. Huc, R. G. Khoury, M. J. Krische, J.-M. Lehn, *Nature* **2000**, *407*, 720–723. For an account, see: references [8a,c].
- [20] Original work by the Li group: a) X. Zhao, X.-Z. Wang, X.-K. Jiang, Y.-Q. Chen, Z.-T. Li, G.-J. Chen, *J. Am. Chem. Soc.* **2003**, *125*, 15128–15139. For an account, see: ref. [8b].
- [21] Original work by the Gong group: B. Gong, Y. Yan, H. Zeng, E. Skrzypczak-Jankunn, Y. W. Kim, J. Zhu, H. Ickes, *J. Am. Chem. Soc.* **1999**, *121*, 5607–5608.
- [22] For stabilizing interactions between *ortho*-alkoxy and H(5)-triazole substituents, see: a) Y.-Y. Zhu, G.-T. Wang, R.-X. Wang, Z.-T. Li, *Cryst. Growth Des.* **2009**, *9*, 4778–4783; b) see: reference 13 g.
- [23] a) J. D. Dunitz, R. Taylor, *Chem. Eur. J.* **1997**, *3*, 89–98; b) Special Issue: Fluorine in the Life Sciences, *ChemBioChem* **2004**, *5*, 557–726.
- [24] For example, see: a) C. Li, S.-F. Ren, J.-L. Hou, H.-P. Yi, S.-Z. Zhu, X.-K. Jiang, Z.-T. Li, *Angew. Chem.* **2005**, *117*, 5871–5875; *Angew. Chem. Int. Ed.* **2005**, *44*, 5725–5729; b) Q. Gan, C. Bao, B. Kauffmann, A. Grelard, J. Xiang, S. Liu, I. Huc, H. Jiang, *Angew. Chem.* **2008**, *120*, 1739–1742; *Angew. Chem. Int. Ed.* **2008**, *47*, 1715–1718; C. Bao, B. Kauffmann, Q. Gan, K. Srinivas, H. Jiang, I. Huc, *Angew. Chem.* **2008**, *120*, 4221–4224; *Angew. Chem. Int. Ed.* **2008**, *47*, 4153–4156.
- [25] a) P. C. Myhre, J. W. Edmonds, J. D. Kruger, *J. Am. Chem. Soc.* **1966**, *88*, 2459–2466; b) J. Hilton, L.-H. Sutcliffe, *Progr. NMR Spect.* **1975**, *10*, 27–39; c) J. W. Emsley, L. Phillips, V. Wray, *Progr. NMR Spect.* **1976**, *10*, 83–756.
- [26] S. T. Howard, *J. Am. Chem. Soc.* **1996**, *118*, 10269–10274.
- [27] A representative example is given in: O. Takahashi, Y. Kohno, M. Nishio, *Chem. Rev.* **2010**, *110*, 6049–6076.
- [28] For photoswitchable foldamers see: a) A. Khan, C. Kaiser, S. Hecht, *Angew. Chem.* **2006**, *118*, 1912–1915; *Angew. Chem. Int. Ed.* **2006**, *45*, 1878–1881; b) A. Khan, S. Hecht, *Chem. Eur. J.* **2006**, *12*, 4764–4774; c) C. Tie, J. C. Gallucci, J. R. Parquette, *J. Am. Chem. Soc.* **2006**, *128*, 1162–1171; d) Y. Wang, F. Bie, H. Jiang, *Org. Lett.* **2010**, *12*, 3630–3633; e) Y. Hua, A. H. Flood, *J. Am. Chem. Soc.* **2010**, *132*, 12838–12840.
- [29] For a leading overview, see: W. F. van Gunsteren, Z. Gattin in *Foldamers: Structure Properties and Applications* (Eds.: S. Hecht, I. Huc), Wiley-VCH, Weinheim, **2007**, pp. 173–192.

Received: August 28, 2010

Published online: December 10, 2010